

TRANSONIC BUFFET AND STATIC AEROELASTIC RESPONSE OF A COMMERCIAL TRANSPORT AIRCRAFT

Michael Candon[1], Truman Gerner[1], Arpan Das[1], Zev Hoffman[1], Pier Marzocca[1], Luke Munholand[2], Valerio Viti[2] & Earl Dowell[4]

[1]RMIT University, Melbourne, AU.
[2]ANSYS Inc., Canonsburg, USA.
[4]Duke University, Durham, USA.

Abstract

Numerical simulation of transonic shock buffet remains a significant challenge in aerospace engineering because of its inherently nonlinear, unsteady, and three-dimensional nature. This is particularly true for full aircraft configurations, where simulations are computationally expensive and their accuracy remains strongly dependent on the turbulence model and numerical setup. As a result, there is still no clear consensus on the most reliable approach for modeling three-dimensional transonic buffeting flows. This paper assesses the efficacy of Unsteady Reynolds-averaged Navier–Stokes (URANS) models for shock buffet on the NASA Common Research Model. Static aeroelastic results are also presented as a step towards full three-dimensional aeroelastic buffet simulations. The results show that It is shown that while some URANS-based models can provide a reasonable prediction of the buffet, robustness and generalizability remains an issue.

Keywords: Unsteady Aerodynamics, Transonic Buffet, Aeroelasticity, Computational Fluid Dynamics

1. Introduction

Transonic shock buffet is a nonlinear unsteady aerodynamic phenomenon, characterized by large amplitude shock oscillations that result from shock wave boundary layer interactions [1]. Shock buffet is a global flow instability, meaning that it occurs even in the absence of structural motion. Although shock buffet occurs only within a narrow window of the transonic regime, it remains a primary contributor to fatigue life degradation, a limiting factor of the flight envelope, and adversely affecting pilot handling and comfort [2]. Further to all this, in the presence of shock buffet, an array of dangerous “flutter-like” aeroelastic instabilities are also possible [3, 4, 5]. While a major driver for transonic buffet research comes from the defense sector, e.g., the F-16 is renowned for its issues with the phenomenon [6], the civil aviation sector also requires careful consideration of its effects. For instance, the sustainable aviation sector is seeing a demand for novel light weight and aerodynamically efficient aircraft designs, requiring that practitioners pay very close attention to dynamic aeroelastic effects in the transonic regime - as highlighted in Boeing’s work on the Transonic Truss-Braced Wing [7].

The aerodynamic aspects of shock buffet on a rigid body have been widely studied, with experimental campaigns dating back to the 1980’s [8], and more recent campaigns considering the two-dimensional (2D) [9] and three-dimensional (3D) [10] buffet mechanism. In the last two decades, exponential growth in computing power and broader access to high performance computing (HPC) have enabled researchers to study the phenomenon numerically using computational fluid dynamics (CFD) codes. Such research was initially dominated by 2D Unsteady Reynolds-Averaged Navier-Stokes (URANS) simulations with mixed success. On one hand, some of the earlier work demonstrated that URANS codes can capture 2D buffet with reasonable accuracy [11] while, on the other hand, generalization remains challenging. For instance, different turbulence models can produce

vastly different results [12]. Most recently, numerical modeling of 3D buffet has seen major interest on wings or half-span aircraft models. In such cases, the limitations of URANS codes are more prevalent, even for simple 3D wings [13]. As a result, scale resolving codes, including variants of Large Eddy Simulation (LES), have seen increased use for buffeting flows, albeit at a massive computational cost, with an up-to-date review provided by Lusher *et al.* [14].

One benchmark configuration that is now widely used for 3D transonic buffet validation is the NASA Common Research Model (CRM), a contemporary transport aircraft geometry originally developed to support the AIAA Drag Prediction Workshop (DPW) in 2007 [15]. The CRM's extensive experimental database across multiple facilities, together with its well-defined public geometry, has made it a standard model for CFD benchmarking of transonic shock motion, separation onset, and the resulting unsteady loads. Of particular relevance to buffet are experimental campaigns conducted by JAXA using an 80% scaled CRM model [10, 16]. In addition to steady forces and moments, the campaign provides time-resolved measurements in buffet conditions, including unsteady surface pressures on the main wing, integrated aerodynamic loads, and wing deformation data. The tests were performed at $M_\infty \approx 0.85$ over angles of attack spanning pre-buffet to fully developed buffet.

This paper presents URANS simulations of transonic shock buffet on the NASA Common Research Model using the stress-ω formulation of the Reynolds Stress turbulence model (RSM-SO). The computed unsteady loads, surface-pressure statistics, and spectral content are assessed against available JAXA experimental data for a fully developed buffet condition. Static aeroelastic results are also presented using PyFSI, providing an intermediate step towards fully coupled three-dimensional aeroelastic buffet simulations.

2. Computational Model

The 80% scaled NASA CRM Wing Body Tail model is used (presented in Fig. 1), which has experimental measurements available from a campaign conducted by the Japan Aerospace Exploration Agency (JAXA) [16]. The design Mach number and lift coefficient of the model are 0.85 and 0.5 respectively. The wing consists of a taper ratio of 0.275, a 25% chord sweep of 35° and an aspect ratio of 9. The model reference area is $A_{textref} = 0.179014\text{m}^2$, the reference chord is $c_{textref} = 0.1531\text{m}$ and the span is $b = 0.26927\text{m}$. Lines of 12 unsteady pressure sensors are located at $\eta = 0.5$ and $\eta = 0.6$, where η is the spanwise location normalized by the semi-span $(b/2)$. This paper considers the experimental test case operating in air with a Mach number of $M_\infty = 0.85$, an angle-of-attack of $\alpha_0 = 4.71°$, a Reynolds number based on the chord length of $Re_c = 2.22 \times 10^6$, and a total pressure of $p_0 = 120kPa$.

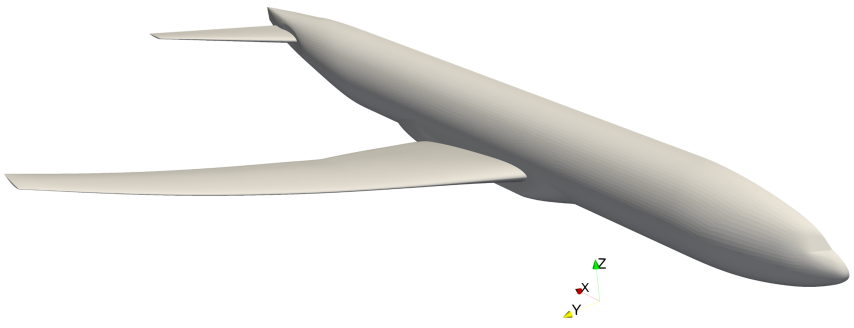


Figure 1 – NASA Common Research Model

3. Computational Framework

3.1 Python Fluid-Structure Interaction (PyFSI)

PyFSI is an in-house CFD-based aeroelastic code developed at RMIT University for the simulation of static and dynamic coupled fluid–structure interaction problems. The framework, as presented in Fig. 2, brings together a range of structural, aerodynamic, gust-response, external-load, and control-load modeling capabilities within a common aeroelastic simulation environment. It supports fully

nonlinear time-marching CFD-based aeroelastic simulations (presently using ANSYS Fluent), as well as CFD-based time-domain and frequency-domain aerodynamic linearization, and CFD-based nonlinear reduced-order modeling capability. In addition, PyFSI can treat gust response problems using either CFD-based or reduced-order aerodynamic models, as well as basic open-loop control inputs. On the structural side, the framework is formulated to couple with general finite-element models, allowing a range of element types and structural discretizations to be used. Methods like fictitious masses and residual vectors are available to correct for localized distortions in modal structural models, e.g., for modeling discrete nonlinear structural mechanisms.

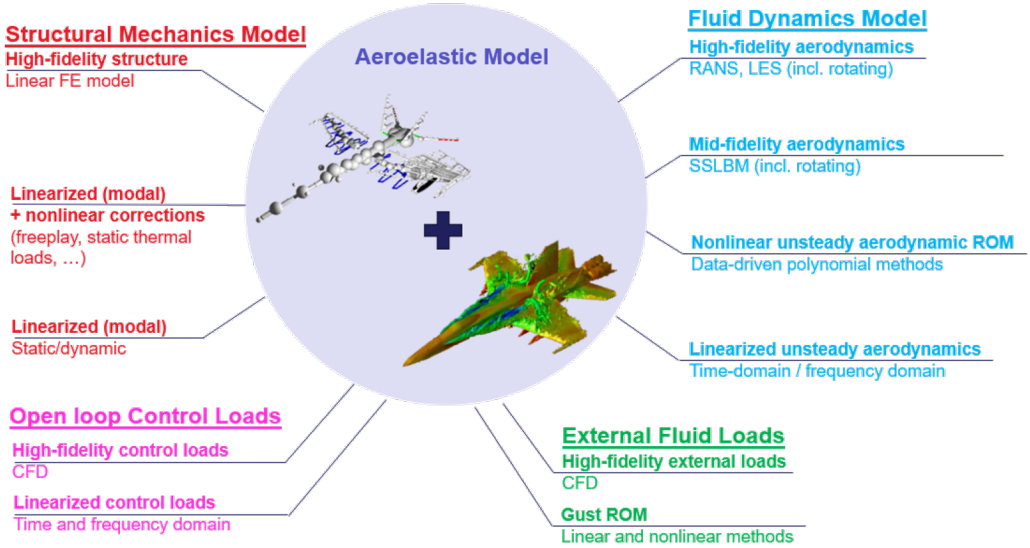


Figure 2 – PyFSI suite of solvers.

3.2 Aeroelastic Equation of Motion

In PyFSI, the structural displacement can be represented in generalized modal coordinates by approximating the physical displacement field as a linear combination of retained mode shapes, $\boldsymbol{v} \approx \boldsymbol{\Phi}\boldsymbol{\xi}$, where $\boldsymbol{\Phi}$ contains the selected structural modes and $\boldsymbol{\xi}$ contains the corresponding generalized modal amplitudes. In these coordinates, PyFSI solves the aeroelastic equation of motion as

$$\boldsymbol{GM}\ddot{\boldsymbol{\xi}} + \boldsymbol{GK}\boldsymbol{\xi} + \boldsymbol{Q} = 0, \tag{1}$$

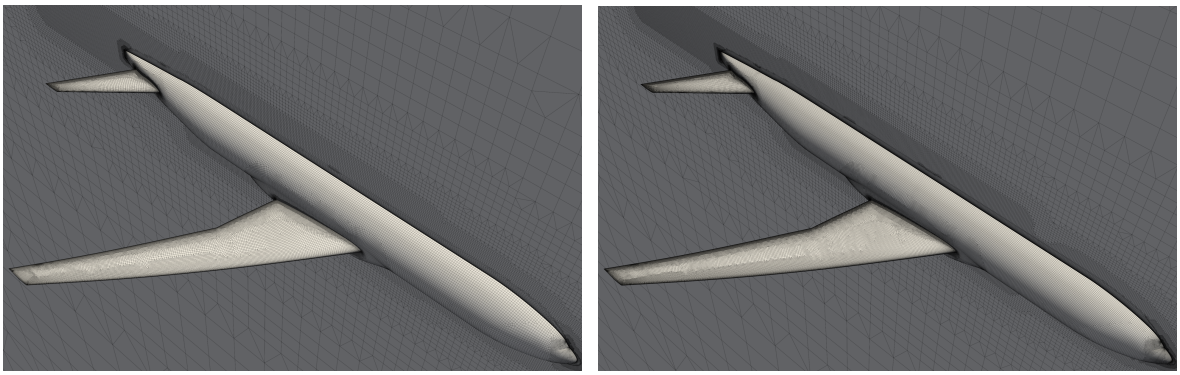
where $\boldsymbol{GM}$ and $\boldsymbol{GK}$ are the generalized mass and stiffness matrices, and $\boldsymbol{Q}$ is the generalized aerodynamic force vector. In the present work, $\boldsymbol{Q}$ is obtained directly from the CFD surface loads and projected onto the structural modal basis. Only the static aeroelastic solution is considered in this paper, such that the acceleration term is zero.

3.3 Computational Fluid Dynamics

The 3D URANS equations for the transient flowfields are solved via a coupled pressure-based solver with implicit second-order spatial discretization for all flow variables, second-order temporal discretization, and Rhie-Chow: distance-based flux interpolation. All simulations were performed using the Stress-ω formulation of the Reynolds-stress turbulence model (RSM–SO model), containing seven additional transport equations: six for the independent Reynolds-stress components and one for the specific dissipation rate, ω. Boundary layer tripping is not considered. A dual time-stepping scheme is used with second-order implicit temporal discretization. A non-dimensional time-step of $\Delta\tau = t(u_\infty/c_ref) = 5 \times 10^{-3}$ is used, where u_∞ is the freestream velocity. Twenty sub-iterations per timestep are considered and all residuals reduce to $\sim 1 \times 10^{-}6 - 1 \times 10^{-}7$. The transient simulation is restarted from a converged steady-state run. Committee supplied grids for DPW8 are used which are generated in Pointwise and available for download [1]. While spatial convergence studies are ongoing,

[1] https://aiaa-dpw.larc.nasa.gov/grids.html

two grids have been used in this paper, denoted by Grid L1-L2, both with an average non-dimensional first cell height of $\bar{y^+} < 1$.



(a) Grid L1: ~ 21M cells (b) Grid L2: ~ 51M cells

Figure 3 – Computational grids for the NASA CRM

3.4 Computational Structural Dynamics

The structural representation is a simplified stick/shell model of the half-span CRM, with shell elements for the wing and horizontal tail and a reduced beam representation of the fuselage. The model is not intended to reproduce the full detailed airframe structure directly; instead, it provides a compact skeleton onto which the mode shapes are mapped. In the aeroelastic solver, the structural motion is then represented in generalized modal coordinates, with physical displacements recovered from the modal basis.

A selection of the CRM wind tunnel model mode shapes, mapped onto the stick/shell model, are shown in Fig 4. While they cannot really be interpreted as a standard modal sequence of aircraft modes, for instance, the first mode is a sting mode and characterized by rigid rotation of the fuselage, while the wing torsion mode does not appear until mode 10, the model remains highly useful for the development and testing of CFD-based aeroelastic codes.

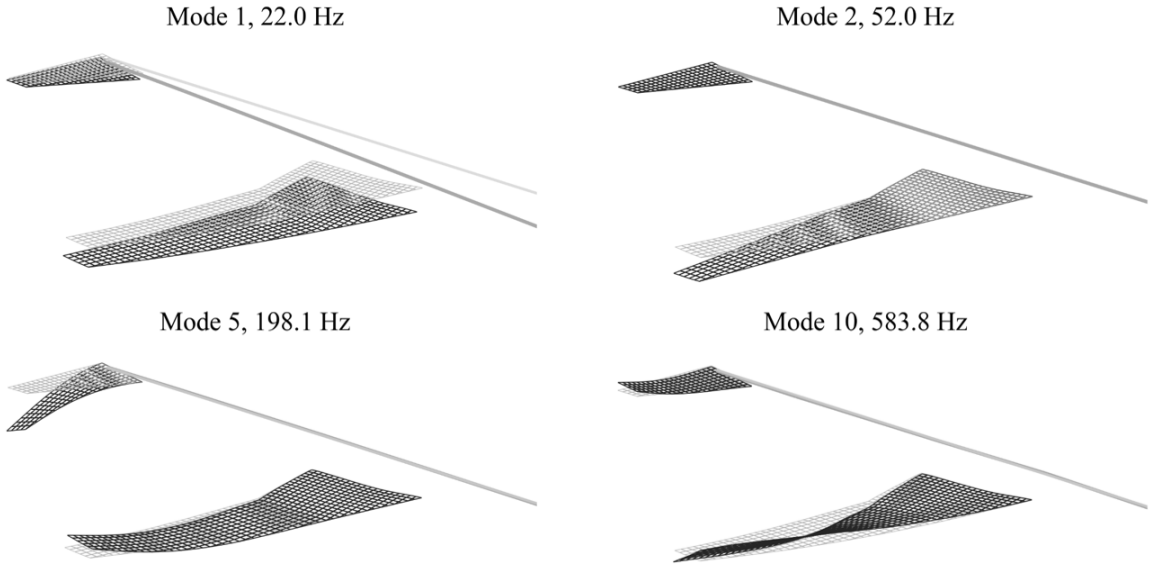


Figure 4 – Mode shapes for the NASA CRM JAXA wind tunnel model.

4. Results

All results consider $M_\infty = 0.85$, $\alpha_0 = 4.71^\circ$, $Re_c = 2.22 \times 10^6$, and $p_0 = 120, \mathrm{kPa}$. In the experimental campaign, buffet was found to be fully developed at this condition. It is important to note that the buffet simulations presented here are performed using the undeformed jig shape. Although the computed static aeroelastic shape is not significantly different from the jig shape, even small changes in the wing shape may be important given the sensitivity of transonic buffet to the mean flow state. Therefore, a more rigorous comparison with the experiment would require simulations about the computed static aeroelastic shape.

Before examining the results, it is worth noting that many variants of the SST $k-\omega$ turbulence model were also tested, including the one-equation intermittency transition model; however, none displayed any noteworthy unsteadiness. This steady behavior was found to be relatively insensitive to the SST variant considered.

In contrast, the RSM-SO model was the only closure tested that produced sustained buffet-like unsteadiness. However, the quality of the resulting mean flow was strongly case dependent. For the lower-Reynolds-number cases (which were also statically deformed), the RSM-SO solutions exhibited buffet, but with excessive wing separation. This was particularly evident at the higher angle of attack, where the separated region was significantly larger than expected. For the higher-Reynolds-number jig-shape case, the RSM-SO solution produced buffet while maintaining a more reasonable mean separated-flow topology. However, this case has not yet been repeated using the statically deformed geometry, for which the spanwise distribution of local angle of attack will differ.

Table 1 – Summary of turbulence-model behaviour for selected CRM buffet cases.

Case	Mach	α_0 [°]	Re_c	CAD	SST k–ω	RSM-SO
1	0.85	4.84	1.515M	static def.	no buffet	buffet; overly separated
2	0.85	5.89	1.515M	static def.	no buffet	buffet; significantly overly separated
3	0.85	4.71	2.270M	jig	no buffet	buffet; good mean separation

Hybrid RANS–LES models, such as Stress-Blended Eddy Simulation (SBES), are presently being investigated and are showing promise.

4.1 Forces and Moments

Figure 5 presents the computed aerodynamic coefficient histories for the RSM–SO simulation on Grid L1. Following the initial transient, the forces develop a sustained periodic response, consistent with a self-excited buffet cycle, with drag clearly exhibiting higher harmonic behavior. The corresponding time-averaged coefficients are shown in Figure 6. The predicted mean lift and pitching moment are in reasonable agreement with the experimental data at $\alpha_0 = 4.71^\circ$, indicating that the RSM–SO model captures the global aerodynamic loading at this condition. The larger discrepancy in the pitching moment is expected, since it is more sensitive to small differences in the pressure distribution, particularly those associated with shock position and separation extent.

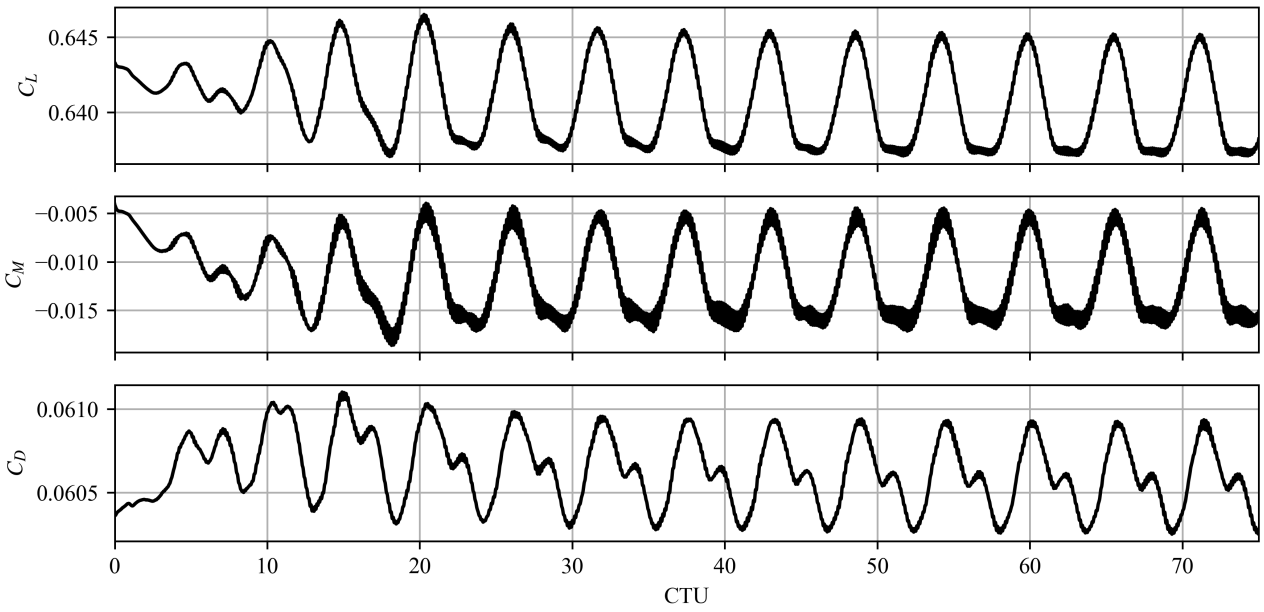


Figure 5 – Time histories of lift, drag and moment coefficients (Grid L1).

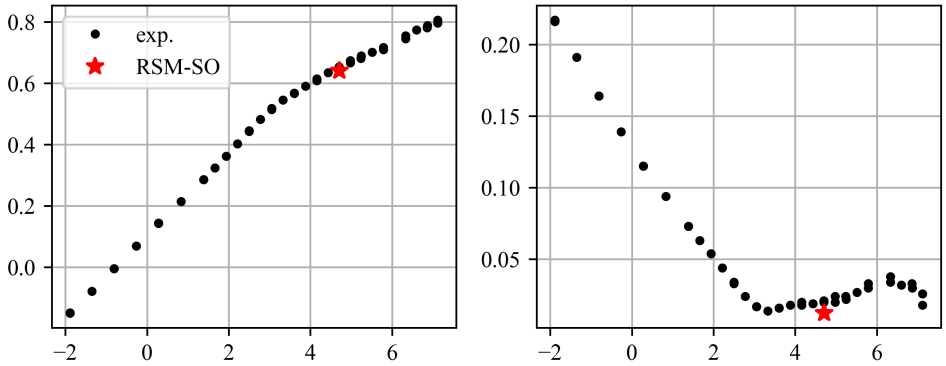


Figure 6 – Time averaged lift and moment coefficients (Grid L1).

4.2 Surface Pressure

The sectional pressure distributions are shown in Figure 7. At both spanwise stations, the RSM–SO simulations reproduce the main features of the measured mean and RMS pressure distributions, including the strong upper-surface shock, the subsequent pressure recovery, the magnitude of the RMS pressure peak, and the approximate extent of the shock excursion. The main differences between the two grids occur in the shock region. Grid L1 generally predicts a slightly broader and more downstream-shifted pressure recovery, particularly in the RMS distributions, where the peak unsteadiness is displaced aft relative to the experimental data. Grid L2 gives a sharper shock and a more upstream-localized RMS peak, which is generally closer to the measured shock-excursion region. This is most evident at $\eta = 0.5$, where the L2 RMS peak aligns more closely with the experimental peak, while the L1 peak is shifted downstream. At $\eta = 0.6$, both grids capture the dominant RMS peak, although L2 again predicts a stronger and more localized response. The L2 result is included to show the trend, although this simulation is not yet fully complete and should therefore be interpreted as preliminary.

The corresponding upper-surface RMS pressure contours are shown in Figure 8. The experiment shows a distinct band of high pressure fluctuation associated with shock motion, extending over the outboard portion of the wing. The RSM–SO simulations reproduce this dominant shock-unsteadiness band and its general spanwise orientation. However, the computed contours are smoother and more

coherent than the experimental field, which contains a more irregular distribution of fluctuation intensity. Grid L2 produces a stronger and more sharply defined RMS band than Grid L1, consistent with the sectional cuts. Overall, the comparison indicates that the RSM–SO model captures the primary shock-motion signature of the buffet, although discrepancies remain in the detailed amplitude and downstream distribution of the pressure fluctuations.

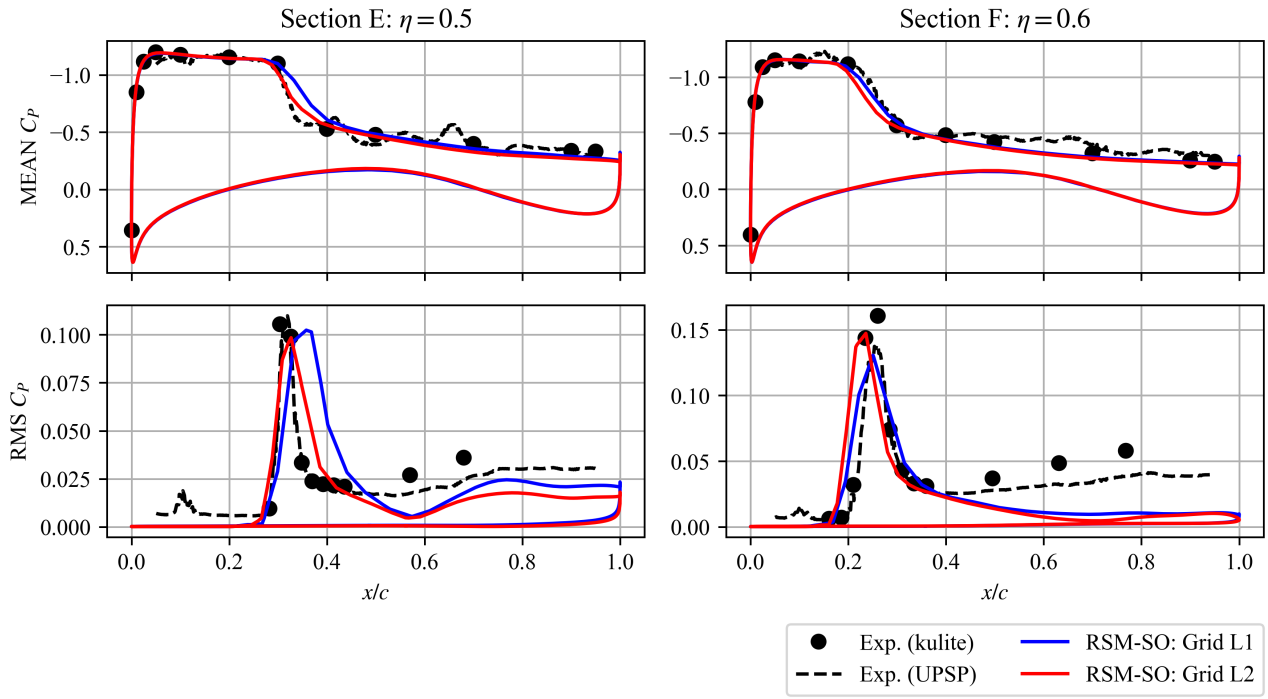


Figure 7 – Sectional pressure coefficient distributions.

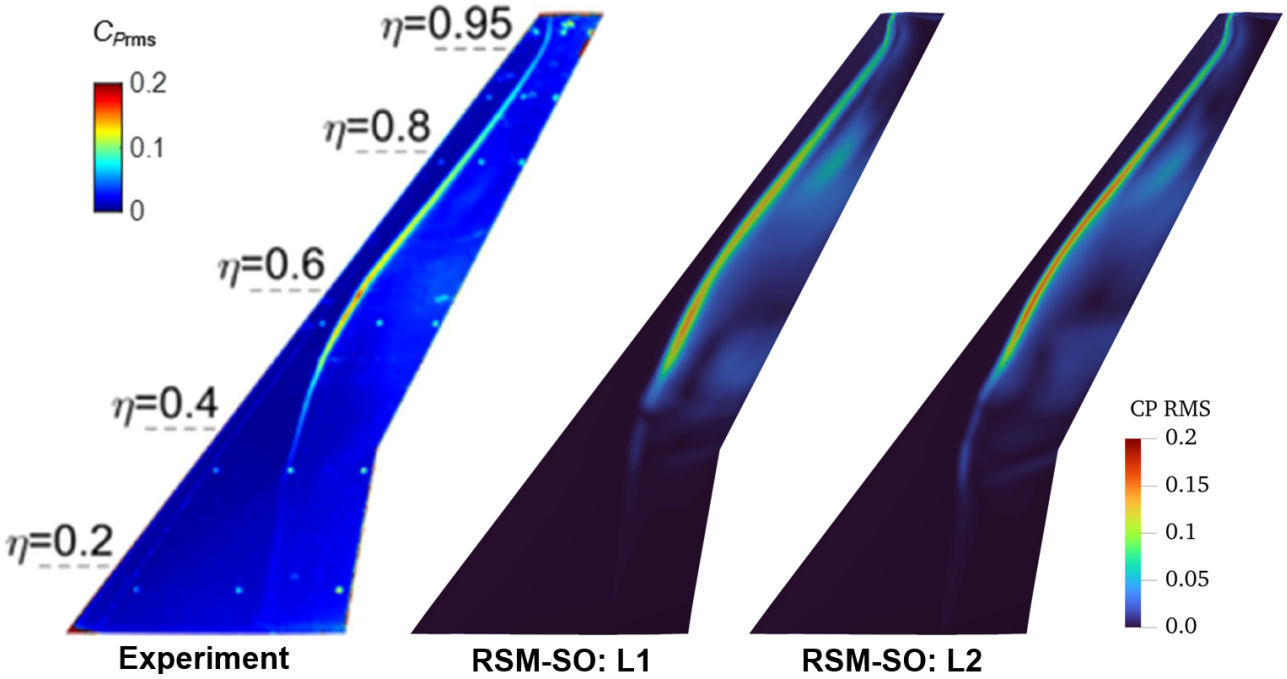


Figure 8 – RMS surface pressure contours on the wing upper surface.

4.3 Spectra

Figure 9 shows the pressure spectra at selected upper-surface locations, corresponding to Kulite location on the experimental model. The CFD-based spectra exhibit a clear dominant peak at ap-

proximately 330 Hz, consistent with the periodic shock motion observed in the force histories. At the upstream locations, $x/c \approx 0.3$, which are closer to the shock oscillations, the spectral energy is stronger. Downstream, the spectral energy is reduced and more broadly distributed, indicating that the strongest coherent unsteadiness is associated with the shock excursion.

The experimental spectrum shown at $\eta = 0.6$ is not taken at the exact same chordwise location as the CFD probe, although it is sufficiently close to provide a useful comparison. The experiment displays a broader-band spectral bump centered at approximately 700 Hz, whereas the present RSM–SO simulation produces a more periodic response at a lower dominant frequency. Therefore, while the simulation captures the presence of shock-related unsteadiness with good prediction of statistic like mean and RMS, the predicted spectral character and dominant frequency are not in close agreement with the experiment.

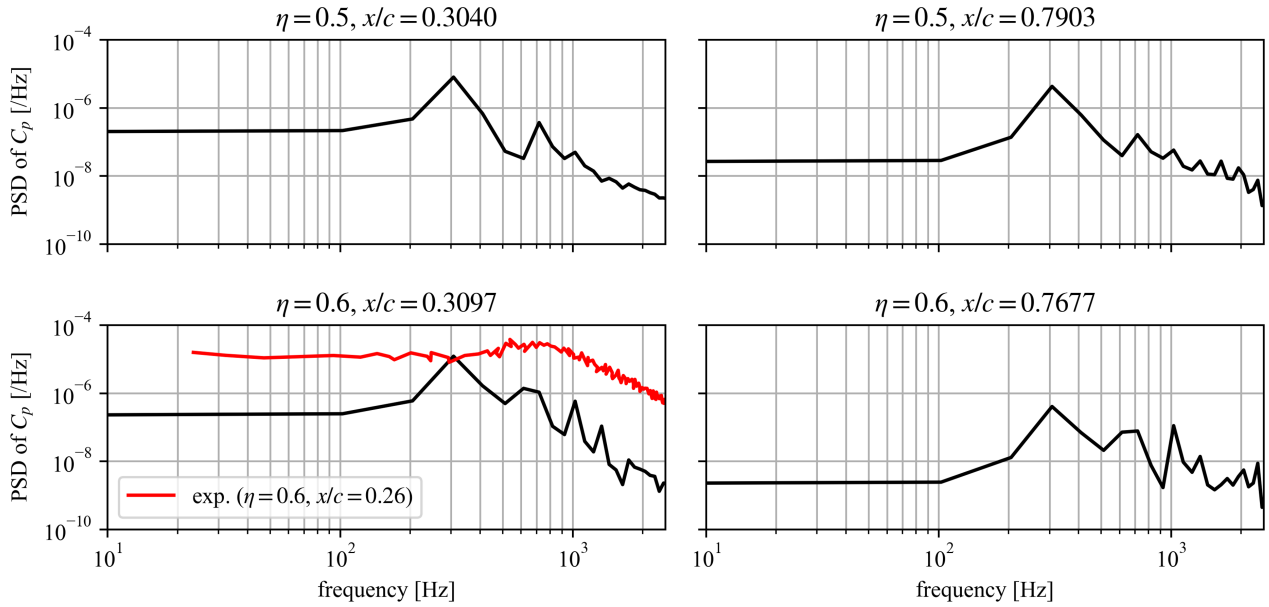


Figure 9 – Power spectral density of instantaneous pressure coefficient at four stations on the wing upper surface.

4.4 Static Aeroelastic Response

The static aeroelastic response was computed using a steady-state RSM–SO simulation coupled to the structural model through PyFSI. The resulting deformation is shown in Figure 10, where the wing exhibits an upward tip displacement of approximately 11 mm. This is in good agreement with the value of approximately 10 mm provided by JAXA for this condition.

The agreement in static tip deflection provides an important verification of the coupled CFD–CSD setup and indicates that the mean aerodynamic loading is being transferred to the structural model with reasonable accuracy. Although the resulting static deformation is not large relative to the overall wing geometry, it may still be important for buffet prediction because transonic buffet is highly sensitive to small changes in the mean shock location, separation extent, and local effective angle of attack. This static aeroelastic shape therefore provides the basis for the next stage of the study, in which the buffet simulations will be repeated on the deformed configuration and fully coupled three-dimensional aeroelastic buffet simulations will be performed.

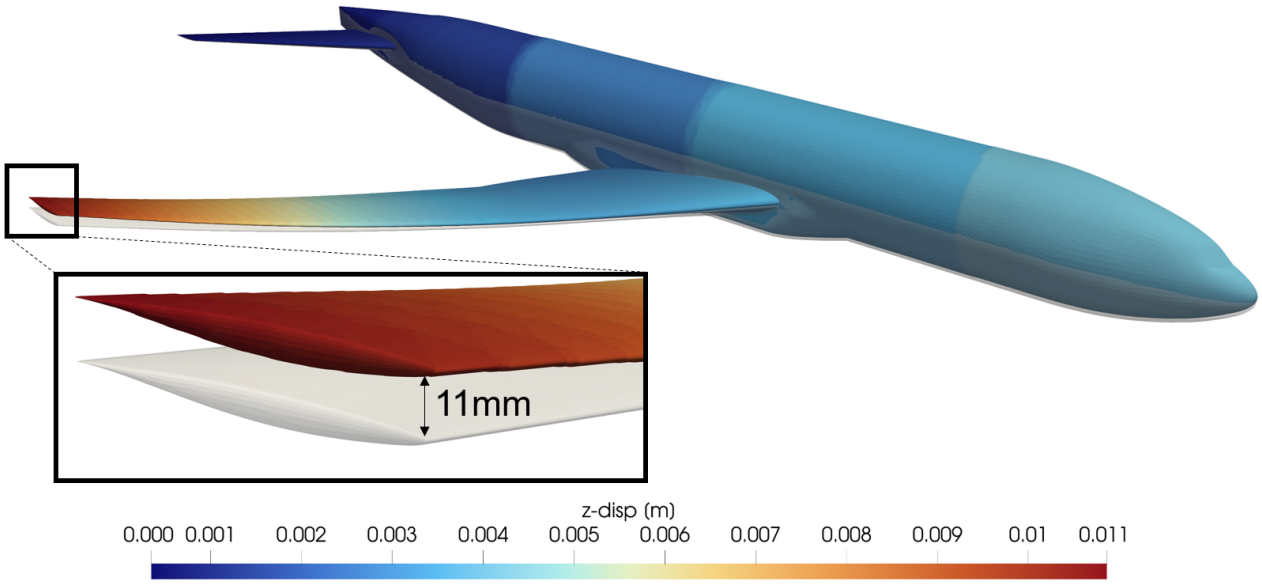


Figure 10 – Computed static aeroelastic deformation of the CRM wing using the steady-state RSM–SO solution.

5. Conclusion

This paper presents URANS simulations of transonic shock buffet on the NASA CRM using the RSM–SO turbulence model. For the fully developed buffet condition considered, the RSM–SO closure is able to produce a sustained unsteady response, whereas the SST k–ω variants tested do not generate comparable buffet behavior. Overall, the results of the RSM-SO model are encouraging, with the predicted mean aerodynamic loads in reasonable agreement with the experimental data. That said, the buffet simulations are still to be run on the statically deformed model. Furthermore, generalization and consistency across operating conditions remains a challenge and requires further assessment. A static aeroelastic simulation is also conducted using PyFSI, and the predicted wing-tip displacement is in good agreement with the value specified by JAXA. This provides a useful basis for the next stage of the work, in which buffet simulations are repeated on the static aeroelastic shape and fully coupled three-dimensional dynamic aeroelastic buffet simulations are performed.

6. Acknowledgments

The authors are grateful for the financial support provided by the Asian Office of Aerospace Research and Development (AOARD) and Air Force Office of Scientific Research (AFOSR), and the ongoing financial support provided by the Australian Defence Science and Technology Group (DSTG). This research was undertaken with the assistance of computing resources from RACE (RMIT Advanced Cloud Ecosystem) and the authors are particularly grateful for the support of Mr Dale Osborne and Dr Robert Shen. Finally, the authors are grateful for the ongoing advice and support of Dr. Walter Silva, Mr Pawel Chwalowski, Dr. Bret Stanford, Dr Brent Pomeroy, Dr Andrea Sansica and all others in the DPW-8/AePW-4 organizing committee.

7. Contact Author Email Address

Dr Michael Candon: candon.michael@rmit.edu.au

8. Copyright Statement

The authors confirm that they, and/or their company or organization, hold copyright on all of the original material included in this paper. The authors also confirm that they have obtained permission, from the copyright holder of any third party material included in this paper, to publish it as part of their paper. The authors confirm that they give permission, or have obtained permission from the copyright holder of this paper, for the publication and distribution of this paper as part of the ICAS proceedings or as individual off-prints from the proceedings.

References

[1] N. F. Giannelis, G. A. Vio, and O. Levinski. A review of recent developments in the understanding of transonic shock buffet. *Progress in Aerospace Sciences*, 92:39–84, 2017.

[2] O. Levinski, D. Conser, C. Mouser, S. Koschel, R. Carrese, M. Candon, , and P. Marzocca. An innovative high fidelity approach to individual aircraft tracking. *AIAA Scitech Forum, AIAA 2020-1647, Orlando, FL*, 2020.

[3] D. E. Raveh and E. H. Dowell. Aeroelastic responses of elastically suspended airfoil systems in transonic buffeting flow. *AIAA Journal*, 52(5):926–934, March 2014.

[4] C. Gao, W. Zhang, X. Li, Y. Liu, J. Quan, Z. Ye, and Y. Jiang. Mechanism of frequency lock-in in transonic buffeting flow. *Journal of Fluid Mechanics*, 818:528–561, 2017.

[5] M. Candon, P. Marzocca, and E. H. Dowell. Aeroelastic reduced-order model differential equations in transonic buffeting flow. *AIAA Journal*, In Press. Pre-Print Available (10.48550/arXiv.2510.22216). 2026.

[6] M. Iovnovich, D. E. Raveh, D. Michaels, and M. Adar. Computational study of transonic limit cycle oscillation phenomenon on f-16 fighter aircraft. *Journal of Aircraft*, 54(2):783–793, 2017.

[7] O. M. F. Browne, D. Maldonado, J. A. Housman, J. C. Duensing, and W. E. Milholen. Predicting transonic buffet onset for the boeing transonic truss-braced wing aircraft. *Journal of Aircraft*, 62(1):62–80, 2025.

[8] J. B. McDevitt and A. F. Okuno. Static and dynamic pressure measurements on a naca0012 airfoil in the ames high reynolds number facility. NASATR NASA-TP-2485, 1985.

[9] L. Jacquin, P. Molton, S. Deck, B. Maury, and D. Soulevant. Experimental study of shock oscillation over a transonic supercritical profile. *AIAA Journal*, 92(9):1985–1994, 2009.

[10] S. Koike, M. Ueno, K. Nakakita, and A. Hashimoto. Unsteady pressure measurement of transonic buffet on nasa common research model. *34th AIAA Applied Aerodynamics Conference*, Washington D.C. 2016.

[11] M. Iovnovich and D. E. Raveh. Reynolds-averaged navier-stokes study of the shock buffet instability mechanism. *AIAA Journal*, 50(4):880–890, 2012.

[12] M. Candon, T. Gerner, P. Marzocca, L. Munholand, V. Viti, and L. Clark. Transonic buffet and stall flutter predictions with a tunable turbulence model for DPW-8/AePW-4. *AIAA Aviation Forum, AIAA 2025-3766*, Las Vegas, NV 2025.

[13] N. F. Giannelis, G. A. Vio, and O. Levinski. Comparison of urans and hybrid rans/les buffet response of the benchmark supercritical wing. *AIAA SCITECH Forum*, National Harbor, Maryland, 2023.

[14] D. J. Lusher, A. Sansica, and A. Hashimoto. Effect of tripping and domain width on transonic buffet on periodic nasa-crm airfoils. *AIAA Journal*, 62(11):4411–4430, 2024.

[15] J. C. Vassberg, M. A. DeHaan, S. M. Rivers, and R. A. Wahls. Development of a common research model for applied cfd validation studies. *26th AIAA Applied Aerodynamics Conference*, Honolulu, HI 2008.

[16] Y. Sugioka, K. Nakakita, S. Koike, T. Nonomura, and K. Asai. Characteristic unsteady pressure field on a civil aircraft wing related to the onset of transonic buffet. *Experiments in Fluids*, 62(1):1–18, 2021.